Journal of
Marine Science and Engineering

MDPI

Article

The Role of Soil Structure Interaction in the Fragility Assessment of HP/HT Unburied Subsea Pipelines

Davide Forcellini [1,*], Daniele Mina [2] and Hassan Karampour [2]

[1] Department of Civil and Environmental, University of Auckland, Auckland 1010, New Zealand
[2] School of Engineering and Built Environment, Griffith University, Gold Coast, QLD 4222, Australia; minad@live.it (D.M.); h.karampour@griffith.edu.au (H.K.)
* Correspondence: dfor295@aucklanduni.ac.nz

Abstract: Subsea high pressure/high temperature (HP/HT) pipelines may be significantly affected by the effects of soil structure interaction (SSI) when subjected to earthquakes. Numerical simulations are herein applied to assess the role of soil deformability on the seismic vulnerability of an unburied pipeline. Overcoming most of the contributions existing in the literature, this paper proposes a comprehensive 3D model of the system (soil + pipeline) by performing OpenSees that allows the representation of non-linear mechanisms of the soil and may realistically assess the induced damage caused by the mutual interaction of buckling and seismic loads. Analytical fragility curves are herein derived to evaluate the role of soil structure interaction in the assessment of the vulnerability of a benchmark HP/HT unburied subsea pipeline. The probability of exceeding selected limit states was based on the definition of credited failure criteria.

Keywords: soil structure interaction (SSI); fragility curves; HP/HT unburied subsea pipelines; numerical simulations; OpenSees

Citation: Forcellini, D.; Mina, D.; Karampour, H. The Role of Soil Structure Interaction in the Fragility Assessment of HP/HT Unburied Subsea Pipelines. *J. Mar. Sci. Eng.* **2022**, *10*, 110. https://doi.org/10.3390/jmse10010110

Academic Editor: José A.F.O. Correia

Received: 23 December 2021
Accepted: 12 January 2022
Published: 14 January 2022

1. Introduction

Assessing the seismic vulnerability of critical infrastructures is fundamental in order to allocate resources toward their design and maintain a certain level of functionality for society. Since pipelines are important networks for servicing communities with water, sewage, oil, and natural gas, decision makers need to carefully preserve their serviceability and resilience. In this regard, buckling is one of the most critical conditions that can lead to severe failure for pipelines and thus was investigated over 30 years. For example, ref. [1] considered the effects of compressive loads due to soil deformability, and [2] analysed the combination of bending and tension by applying a 2D model. Refs. [3–5] performed several parametric studies to assess the axial strains and displacements of pipelines. Recently, ref. [6] developed fragility curves that account for the interaction between buckling and earthquakes, and [7] performed 3D numerical simulations of a partially embedded (unburied) pipeline in to assess its vulnerability to a fault rupture. Other authors (such as [8–13]) investigated the stability of subsea pipelines and pipe-in-pipe systems under hydrostatic, hydrodynamic, thermal, and combined actions. Recently, ref. [14] reviewed several contributions on offshore pipelines suffering buckling due to different reasons (i.e., soil weight, burial depth, axial resistance, imperfection amplitude, temperature difference, interface tensile capacity, and diameter-to-thickness ratio on the uplift and lateral resistance; and the failure mechanism of the pipeline). Moreover, ref. [15] showed a broad overview and discussion of uplift and lateral buckling on buried and partially buried pipelines.

However, very few contributions have considered the effects of SSI on unburied pipelines that have been performed with finite element models. The surrounding soil has been reproduced with several approaches by applying non-linear translational springs [16–20] or 3D solid elements, [21]. In particular, [16] modelled the pipeline with beam elements and represented the soil with discrete nonlinear springs by deriving a formulation to model the pipeline ends with equivalent springs. The role of soil deformability was considered by [22] to study the mutual behaviour (rock and soil layers) of the ground and the pipeline by performing a finite element model and by [23] that investigated the role of fault displacements on the buckling mechanism of buried offshore pipelines in sandy soils. In particular, the mutual soil–pipe interaction may have important effects on the pipeline response, as shown in [24]. Additionally, ref. [21] applied contact elements to describe the SSI, while [25] performed a model that was built up as a combination of elastic theories for both the soil and the beam.

Moreover, [19] performed a finite element model that applies shell elements and springs to assess the axial strains of the pipeline. Furthermore, ref. [26] proposed to model the pipeline with a solid-element model to study strain conditions induced by soil liquefaction. Refs. [19,20,27] modelled the soil with nonlinear springs, while more recently, ref. [28] investigated the interaction between the soil and the pipeline by performing an elastoplastic 3D model. In order to address the gap in the literature, the current work aims to apply the 3D model proposed in [6] to consider the entire system (soil + pipeline) and thus provide more insight into the failure of a subsea pipeline by investigating the effect of soil properties. The performed case study shows the importance of considering the role of SSI on the assessment of the mutual behaviour of soil deformability and structure buckling under seismic scenarios. In particular, neglecting SSI may considerably undervalue the pipeline vulnerability, leading to un-conservative predictions and designs. It is worth noting that the performed numerical model may be useful for further research in marine structures that, upon collapse, may induce large environmental, life, and asset losses, as shown in [29,30]. In addition, some contributions [31,32] investigated the modelling of interactions between saturated and unsaturated soils and cylindrical objects such as pipes. Moreover, ref. [33] investigated the soil resistance during large lateral movements of pipelines across the seabed with particular focus on the analysis of the thermal and pressure-induced expansions.

2. Numerical Model

The seismic assessment of a pipeline performed with numerical simulations was the scope of the previous work [6] that neglected to consider the role of SSI. The present paper considers the same subsea nigh pressure/high temperature (HP/HT) pipeline on the seabed and resting on a sleeper (Figure 1). Table 1 shows the parameters selected for the case study. In [6], two scenarios were analysed: (1) the seismic assessment of a laterally buckled pipe was considered, and (2) the seismic motion was applied at the pipeline subjected to a temperature slightly below the lateral buckling temperature. By developing analytical fragility curves, ref. [6] showed that the probability of failure (exceedance of the yield stress or local buckling of the pipe wall thickness) is higher for scenario 1. In the current study, the same conditions of scenario 1 were considered, and several earthquakes were applied to a comprehensive 3D numerical model performed with OpenSees in order to realistically represent the non-linear behaviour of the soil (such as amplifications, plastic deformations, and permanent movements). Transmitting boundaries were considered at the base to dissipate the radiating waves and to accurately model the damping by preventing the reflection of the seismic waves back into the soil medium after being incident on the far-off boundaries. Lateral boundaries were modelled by adopting the penalty method (tolerance: 10^{-4}) to avoid problems associated with the equations system conditions. Vertical directions were restrained while longitudinal and transversal directions were set free to allow soil shear deformations. The performed soil mesh (200 m $\times$ 200 m, 25 m depth, Figure 2) was selected with a convergence study between several meshes that allowed to select the one presented herein. It is built up with 7450 modes and 6430 non-linear solid brick elements called “Bbar brick” [34,35]. These dimensions have been determined following the suggestions already applied in [36–38], and the discretisation was built up with relatively small elements around the pipeline and gradually larger toward the outer mesh boundaries. The wave propagation is realistically represented by adopting transmitting boundaries located (at 100 m from the centre of the mesh) as far as possible from the pipeline to decrease any effect on the response. In particular, base and lateral boundaries have been modelled to be impervious to represent a small section of a presumably infinite (or at least very large) soil domain and to allow the seismic energy to be removed from the site itself [36–39]. In order to validate these assumptions, the mesh was verified by comparing the acceleration at the top of the mesh with those calculated for free field (FF) conditions.

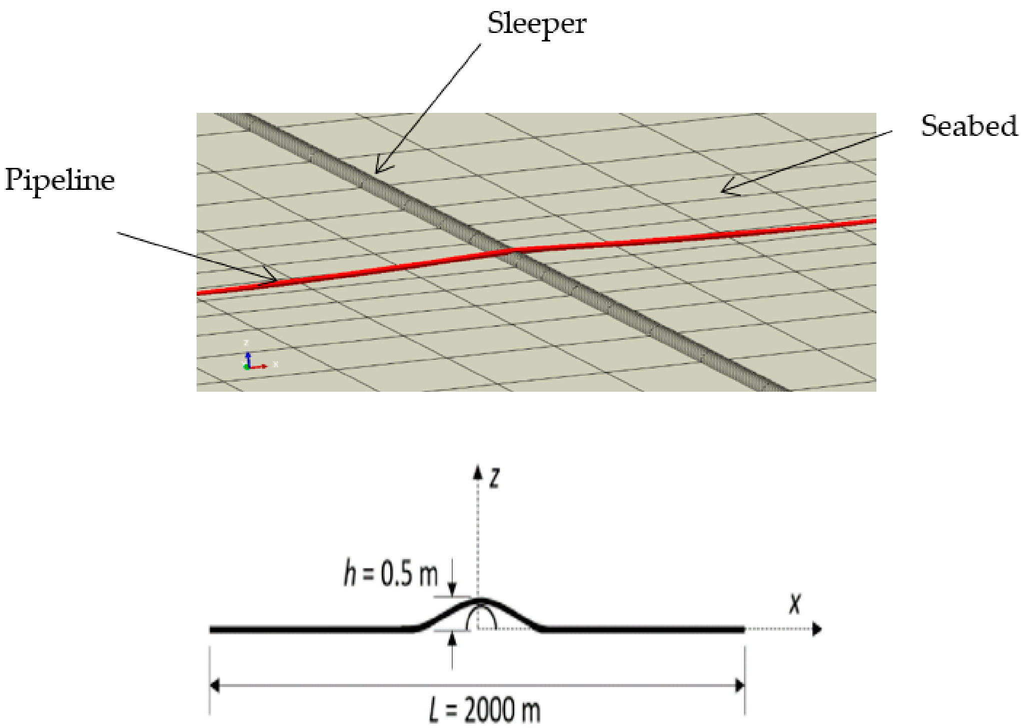

Figure 1. Pipeline and sleeper model used in the thermal buckling and seismic/thermal interaction analyses.

Table 1. Pipeline and seabed properties.

Property	Value
Length, L (m)	2000
Outer diameter, OD (mm)	254
Wall thickness, t (mm)	12.7
Thermal expansion coefficient, α (°C^{-1})	1.01×10^{-5}
Young's modulus, E (MPa)	206,000
Poisson's ratio, ν	0.3
Lateral imperfection ratio, $h_0/l0$	0.012
Submerged weight, q (N/m)	1500
Seabed friction coefficient, μ_1	0.5
Sleeper friction coefficient, μ_2	0.3
Sleeper height, h (m)	0.5

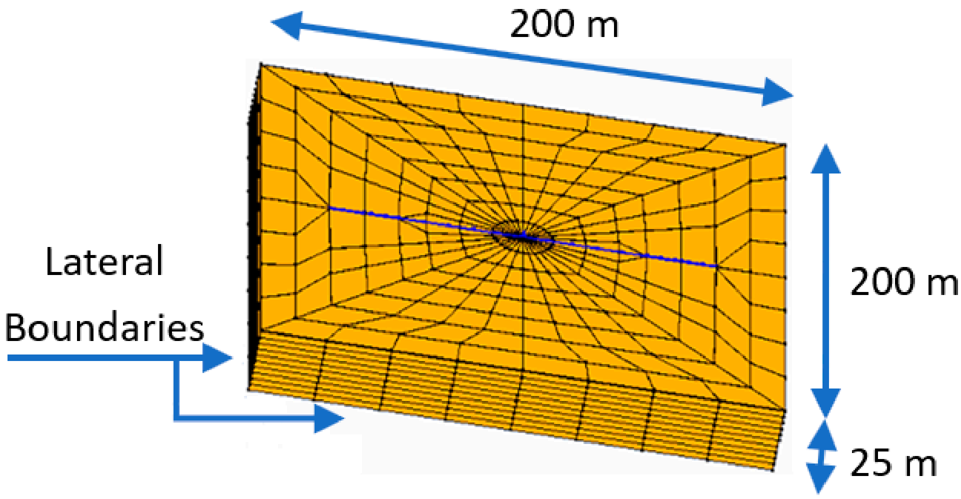

Figure 2. The finite element mesh (indications: dimensions and lateral boundaries).

The soil is performed with a PressureIndependMultiYield (PIMY) model [34], based on the multisurface-plasticity theory for cohesive soils to realistically represent non-linear mechanisms of hysteresis and radiation damping in the ground [35]. This model is implemented in OpenSees to perform monotonic or cyclic response of soils and consists of an elastic–plastic material in which (1) plasticity exhibits only in the deviatoric stress-strain response, (2) the volumetric stress–strain response is linear elastic and independent of the deviatoric response. (3) Plasticity is formulated based on the multi-surface (nested surfaces) concept, with an associative flow rule, and (4) the yield surfaces are assumed to be of the von Mises type. In particular, the load application is defined in two steps: (1) gravity load: the material behaviour is set up as linear elastic. (2) Dynamic (seismic load): the stress–strain response is considered elastic–plastic. The non-linear behaviour of the model is defined with hyperbolic backbone curves that model the relationship between the shear strains and the shear stresses by defining several parameters (shear modulus, bulk modulus, cohesion, and shear wave velocity) for the three homogeneous soil layers (named SOIL1, SOIL2, and SOIL3) that were considered in the study. Figure 3 shows the non-linear backbone curves, represented by hyperbolic relations, while the adopted parameters (see Table 2) have been selected to represent clays with increasing deformability (see [38]).

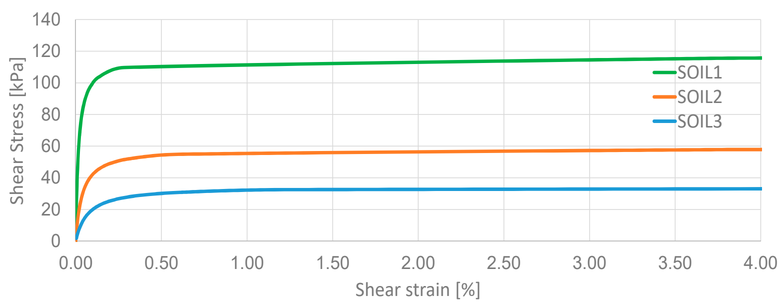

Figure 3. Backbone curves.

Table 2. Soil parameters.

	SOIL1	SOIL2	SOIL3
Mass density (Mg/m^3)	2.0	1.7	1.5
Shear Modulus (kPa)	7.2×10^5	1.53×10^5	6×10^4
Bulk Modulus (kPa)	1.56×10^6	3.32×10^5	3×10^5
Cohesion (kPa)	100	50	37
Shear wave velocity (m/s)	600	300	200

In order to simulate the behaviour of a 2000 m-long pipeline, zero-length elements (in three directions) are used to represent the boundary conditions at the ends of the pipeline. The properties of such elements along the longitudinal and transversal are defined as elastic perfectly plastic (EPP) to reproduce the resistance of the pipeline. The elastic spring that models the vertical direction is calculated on the basis of the soil vertical stiffness. The pipeline was modelled as an isotropic bilinear material (yield stress: σy = 448 MPa and tangent modulus: Et = 2100 MPa). The strains were calculated at the central point, at the crown of the buckled pipeline, [6] and then compared to the failure criteria outlined in the next section. Following [6], the behaviour of the pipeline was calculated with a quasi-static analysis that includes geometric non-linearity and was applied with several time steps to the buckled configuration, namely scenario 1. Several load steps were applied: (1) the self-weight was first applied as a distributed mass (153 kg/m), and then (2) internal pressure (Pint = 12 MPa) was considered and (3) a uniform temperature of 31 °C applied to the wall thickness. As shown in [40,41], the lateral buckling depends on the axial forces in the wall thickness that occur as a consequence of the soil reaction to the deformations when the pipeline is subjected to internal pressure and thermal loading. In this regard, simulating SSI becomes fundamental to realistically predicting such conditions that may severely damage the pipeline. The seismic inputs were applied at the base of the soil domain (25 m depth) in the transversal direction. It is worth noting that the use of a 3D mesh is fundamental in order to account for the deformations in the other directions (longitudinal and vertical) due to the application of the seismic scenario.

It is worth noting that the analysis assumed that no pore water pressure is generated in soils, i.e., the soil is idealised as a single-phase material. The assumption may lead to inaccuracy if liquefaction or other failure mechanisms induced by pore water pressure are important [42,43]. To avoid complexities, the model considers that the flow rule and softening/hardening are independent of stress-induced anisotropy and the magnitude of confining pressure. Nonetheless, these two assumptions are challenged by many studies [42,44,45]. Both assumptions can be relaxed in future studies to increase the accuracy of the prediction by considering more advanced models performed in OpenSees, such as [46,47].

3. Pipeline Failure Criteria

In the technical literature, ref. [48] outlines the local buckling under combined loading failure criteria. The presented case study consists of a pipeline subjected to longitudinal seismic loads. The resulting bending moment, axial force, and internal overpressure (internal pressure due to the external hydrostatic pressure) cause longitudinal strain that needs to satisfy the following design conditions at all cross-sections:

$$\varepsilon_{Sd} \leq \varepsilon_{Rd} = \frac{\varepsilon_c}{\gamma_\varepsilon} \tag{1}$$

$$\varepsilon_c = 0.78(\frac{t}{D} - 0.01)(1 + 5\frac{p_i - p_e}{p_b \cdot \frac{2}{\sqrt{3}}})\alpha_h^{-1.5}\alpha_{gw} \tag{2}$$

where ε_{Sd} is the design compressive strain, p_i and pe are the internal and external pressures, respectively, and γ_ε is the resistance strain factor. The burst pressure p_b is calculated from:

$$p_b = \frac{2t}{D - t} f_Y \frac{2}{\sqrt{3}} \tag{3}$$

The strain hardening parameter αh is equal to 0.93 for the C– Mn steel pipe [48], and the girth weld factor (α_{gw}) is equal to 1 with D/t = 20. For the pipe studied herein with parameters represented in Table 1, ε_c is equal to 0.06.1 mm/mm. The resistance strain factor γ_ε for three different classes, low, medium, and high, are equal to 2.0, 2.5, and 3.3, respectively [48]. The design compressive strain ε_{Sd} for different classes are represented in Table 3. The strain at failure (local buckling of the compressive side) from the FE analysis [6] is also given in Table 3. Fragility curves were applied in order to consider a probabilistic-based methodology that may consider the mutual interaction between soil deformability and the behaviour of HP/HT unburied subsea pipelines. In this regard, ref. [49] proposed a methodology for the derivation of fragility curves for existing structures. In the present paper, fragility curves were developed by considering predefined limit states (LS) of the maximum strains (Table 3) at which the probability of exceedance was calculated. The seismic scenario consisted of 17 input motions with different intensity measures (IMs) in order to assess a wide range of damage in the pipeline (more details in [6]). Figure 4 shows the spectra of the selected 17 input motions and the corresponding peak ground accelerations (PGAs), while the characteristics of the inputs are shown in Table 4. The compression at the crown of the pipeline was considered as the reference parameter to express the damage condition.

Table 3. Failure criteria for different safety classes.

			ε_{Sd} (mm/mm)		
OD (mm)	**t (mm)**	f_Y **(MPa)**	**Low Safety Class**	**Medium Safety Class**	**High Safety Class**
254	12.7	448	3.0×10^{-2}	2.44×10^{-2}	1.85×10^{-2}

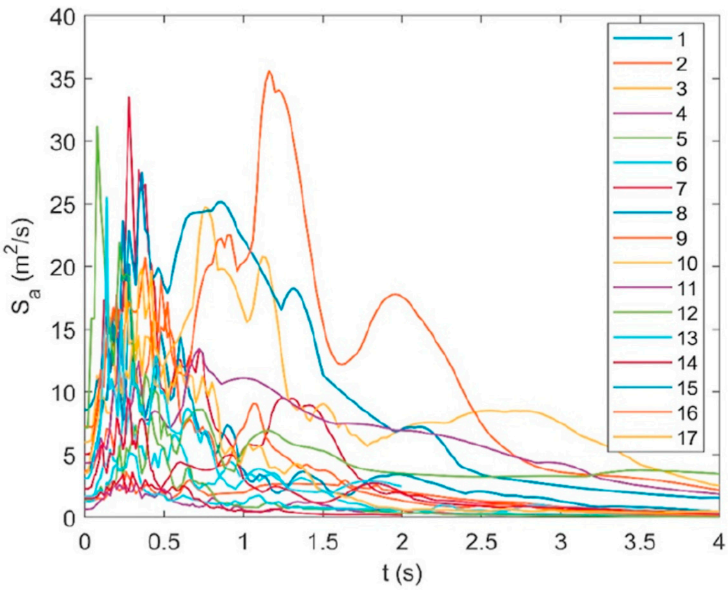

Figure 4. Seismic scenarios.

The results of the analyses were calculated for the three models (SOIL1, SOIL2, and SOIL3) for the 17 selected input motions by considering the peak ground acceleration (PGA) of the earthquake record as the representative intensity measure. The assumptions herein are that the uncertainties of the results may be represented by lognormal distributions, and two parameters were calculated: the logarithmic mean (μ) and standard deviation (β) of the lognormal seismic intensity measure.

Therefore, the results were used to develop linear regressions and to determine the values of the mean and the log-standard deviation. The probability of exceedance (PE) was then calculated as:

$$\mathrm{PE}[D \geq Ci|PGA] = \phi\left(\frac{\ln(PGA) - \mu}{\beta}\right)$$

where PE is the probability of the structural damage (D) to exceed the ith damage state (C), while ϕ is the standard normal cumulative distribution function (more details in [38,39]).

Table 4. Seismic scenario.

Input Motion	Station	PGA [g]	Duration [s]
1	BORREGO	1.24	40.00
2	AZE	1.66	40.00
3	CAP	5.01	40.00
4	CNP	3.53	25.00
5	H-PVB	3.68	40.00
6	SCS	6.00	40.00
7	BLC	0.66	40.00
8	H-COS	1.44	40.00
9	H-CAL	1.26	40.00
10	A-KOD	1.51	21.00
11	Northridge	8.57	15.00
12	Takatori	7.20	40.00
13	Llolleo	3.54	116.50
14	Erzican	4.33	18.00
15	Lucerne Valley	7.12	40.00
16	Imperial Valley	3.09	22.00
17	Trinidad	2.28	21.40

4. Results and Discussion

The first step was to validate the numerical model by comparing the fixed-based results calculated in the previous paper [6] with those obtained herein for SOIL1 in terms of PGA and maximum stress. This comparison shows that both models have the same response under rigid soil conditions (Figure 5), demonstrating a good agreement and thus validating the model assumptions. Then, the response of the rigid soil (with no SSI) that resulted for SOIL2 and SOIL3 was compared (Figure 6), and linear regressions were applied to calculate the mean and the log-standard deviation (Tables 5–7) of the results of the performed non-linear dynamic analyses (for each soil conditions). It is worth noting that deformable soils (SOIL2 and SOIL3) show smaller mean values than those for SOIL1, underlining the effect of soil deformability in reducing the stresses inside the pipeline and thus reducing the global vulnerability. It is the consequence of the deformability of the soil that behaves as a natural isolator for the pipeline.

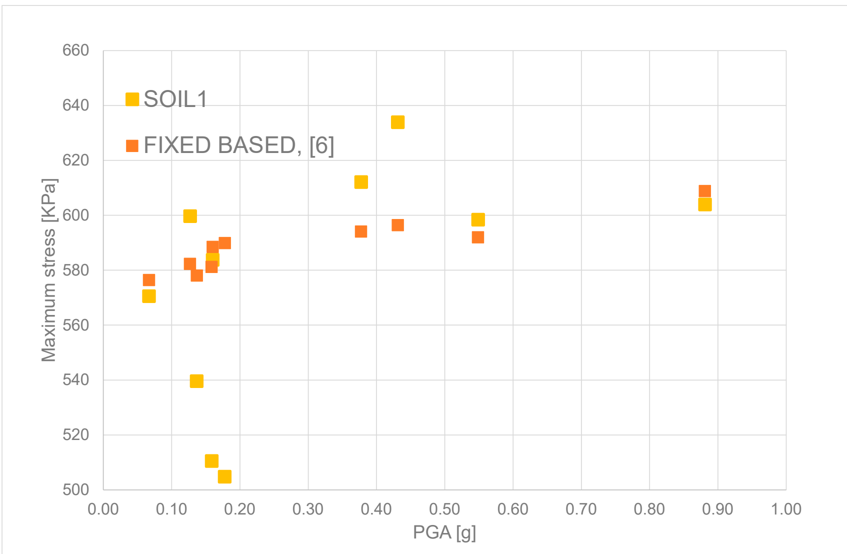

Figure 5. Comparison between results from Soil 1 and fixed based model.

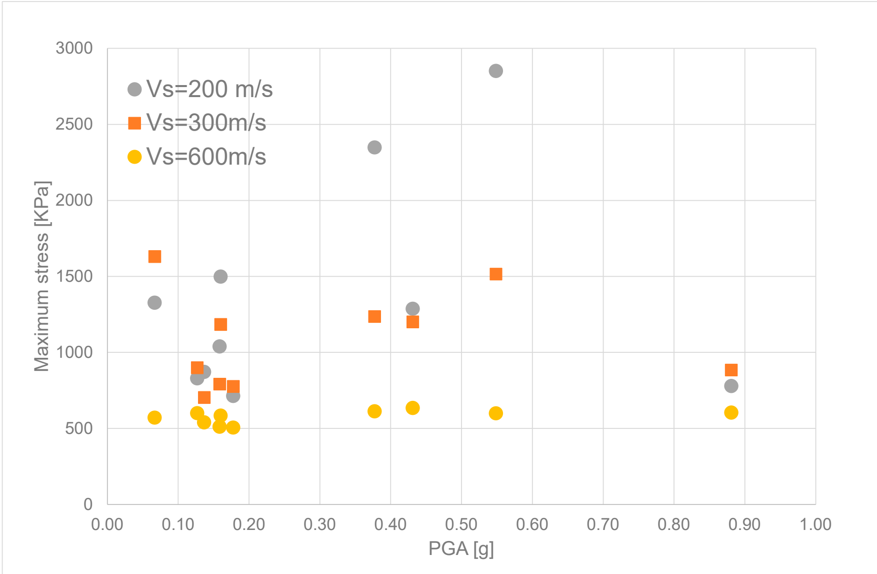

Figure 6. Comparison: SSI effects.

Table 5. Lognormal standard deviation (β) and median (μ) values of SOIL1 at limit states (LSi).

SOIL1	LS1	LS2	LS3	LS4
β	0.793	0.809	0.821	0.833
μ	0.165 g	0.176 g	0.196 g	0.207 g

Table 6. Lognormal standard deviation (β) and median (μ) values of SOIL2 at limit states (LSi).

SOIL2	LS1	LS2	LS3	LS4
β	0.776	0.781	0.791	0.799
μ	0.156 g	0.169 g	0.183 g	0.196 g

Table 7. Lognormal standard deviation (β) and median (μ) values of SOIL3 at limit states (LSi).

SOIL3	LS1	LS2	LS3	LS4
β	0.749	0.728	0.670	0.705
μ	0.144 g	0.149 g	0.158 g	0.168 g

SOIL1 and SOIL2 (Figures 6 and 7) show different fragility curves for the considered limit states: the probability of exceedance (PE) increases with the considered limit state. For SOIL3 (Figure 8), the fragility curves for the various limit states do not differ from each other, since the probability of exceedance (PE) is high even at a slight and moderate level of damage. The performance of the system (soil and pipeline) is shown to be characterised by different levels of PE and, consequently, damage for SOIL2 and SOIL3. SOIL1 represents the case of stiff soil (bedrock conditions), and thus, it may be assumed that SSI effects are negligible (fixed conditions). This aspect may lead to the fact that the pipeline strains are not due to the soil residual plastic deformations, as shown in [6].

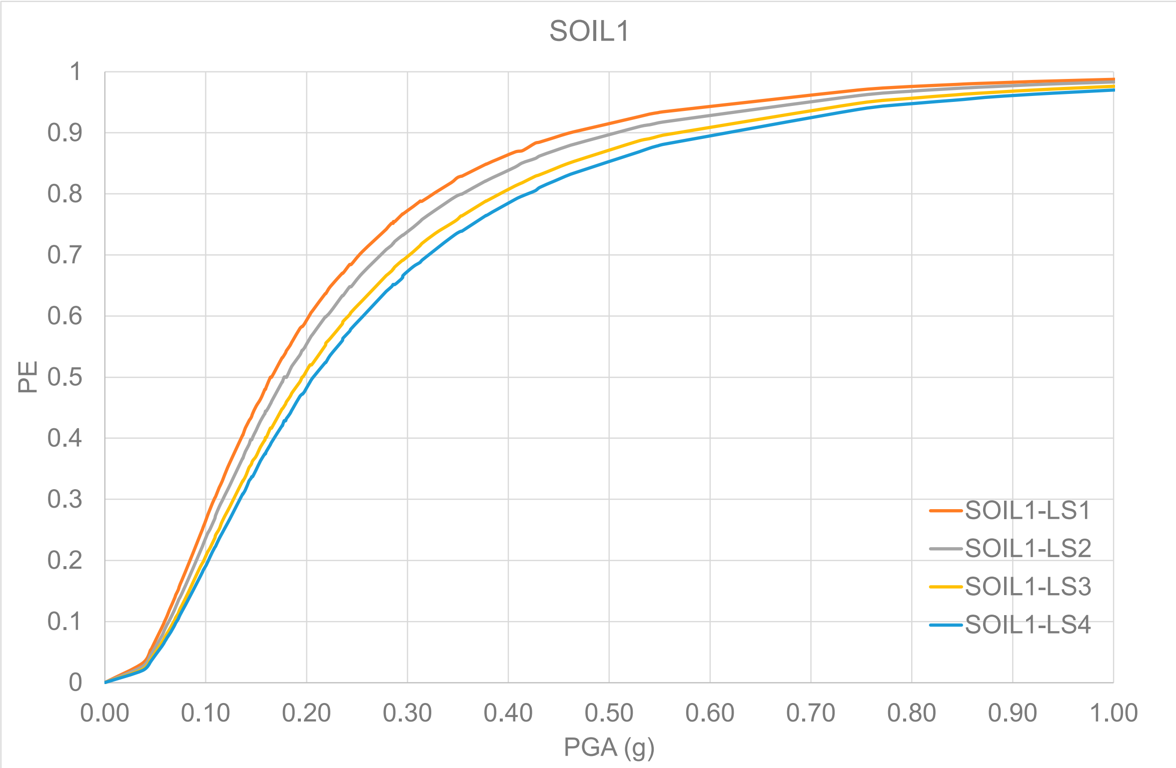

Figure 7. Fragility Curves: SOIL1.

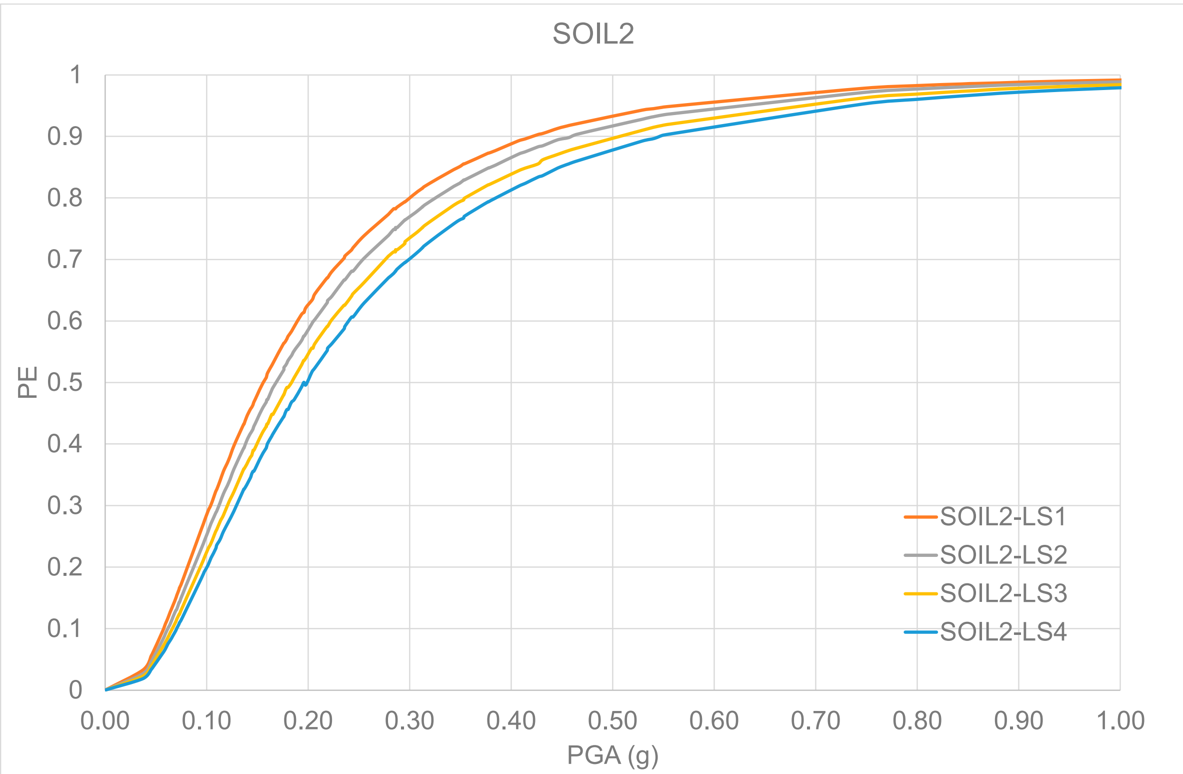

Figure 8. Fragility Curves: SOIL2.

Figures 9 and 10 compare the considered soil conditions for LS1 and LS4, respectively. For example, at 0.30 g (Table 8), PE values for LS1 are 0.77, 0.80, and 0.84, while for LS4, PE values are 0.68, 0.70, and 0.79, respectively, for SOIL1, SOIL2, and SOIL3. In particular, Figures 10 and 11 show that the pipeline vulnerability increases with soil deformability, since at every damage state, the PE for SOIL1 is smaller than those calculated for SOIL2 and SOIL3 for all PGA values. It is worth noting the difference in the probability reached at LS4 for SOIL2 and SOIL3. This difference is relatively small for PGA < 0.20 g and PGA > 0.30 g, while it increases gradually between 0.20 g and 0.30 g. At 0.24 g, the PE values are 0.60 and 0.70 for SOIL2 and SOIL3, respectively. The difference between the two soil conditions decreases for higher intensities and, for example, at 0.70 g, PE values are 0.97 and 0.94. This is due to non-linear deformations in the soils that become significant after a certain level is reached. In particular, the non-linear behaviour of the soil is driven by the ultimate strength of the soil (defined by the backbone curves, Figure 2) that needs a certain level of intensity to be mobilised. For SOIL3, the final shear strength (38 kPa, Figure 2) may be reached for intensity levels that are lower than those for SOIL2 (59.8 kPa, Figure 2). Therefore, the relative damage of the two soil conditions differs mainly at a moderate level of PGA because such intensities may affect the soil in different ways. At a higher level of PGA, the soil mobilises plastic behaviour, and the performance of the soil–pipeline system is similar. Figures 8 and 11 show that the system becomes more fragile due to the damage due to soil deformability. This increased vulnerability is evident for LS4, where SOIL3 shows larger values of PE, demonstrating that SSI effects are detrimental. In particular, the effects of soil damping are significantly important, as shown in [35].

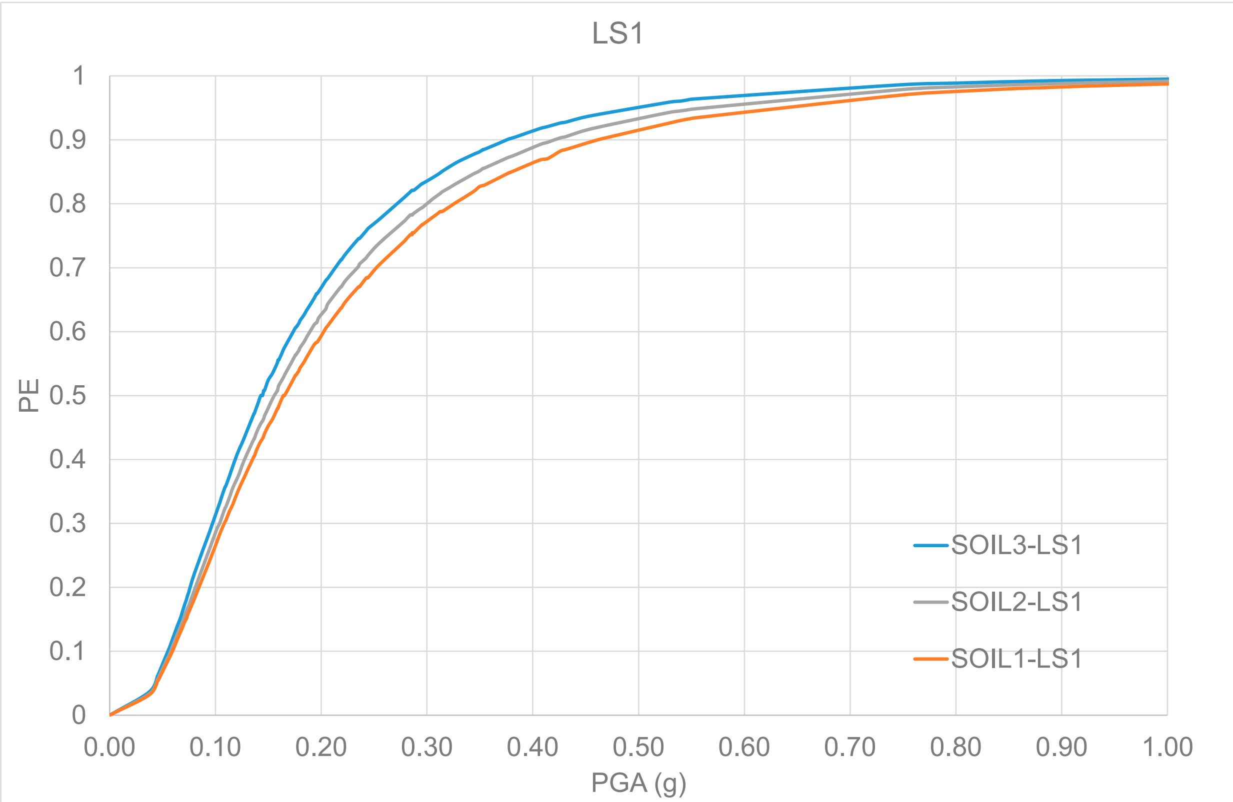

Figure 9. Fragility Curves: comparison LS1.

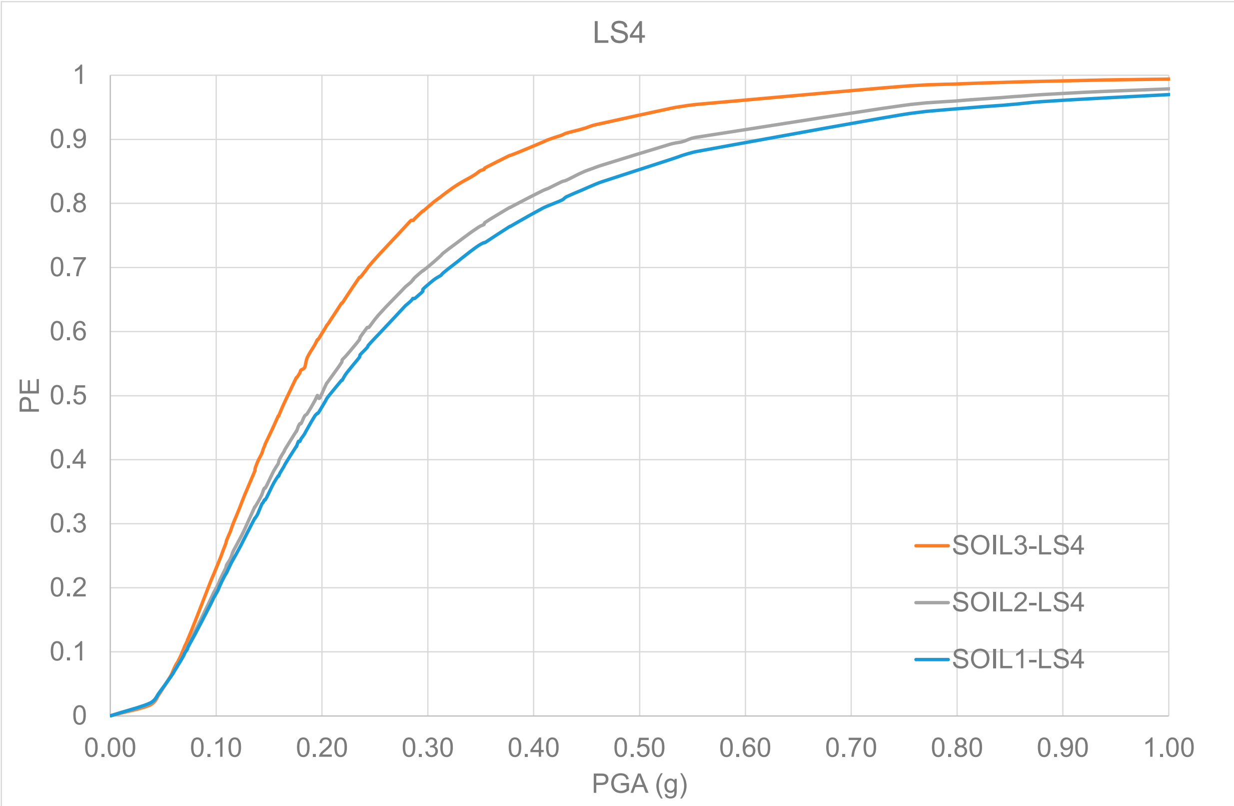

Figure 10. Fragility Curves: comparison LS4.

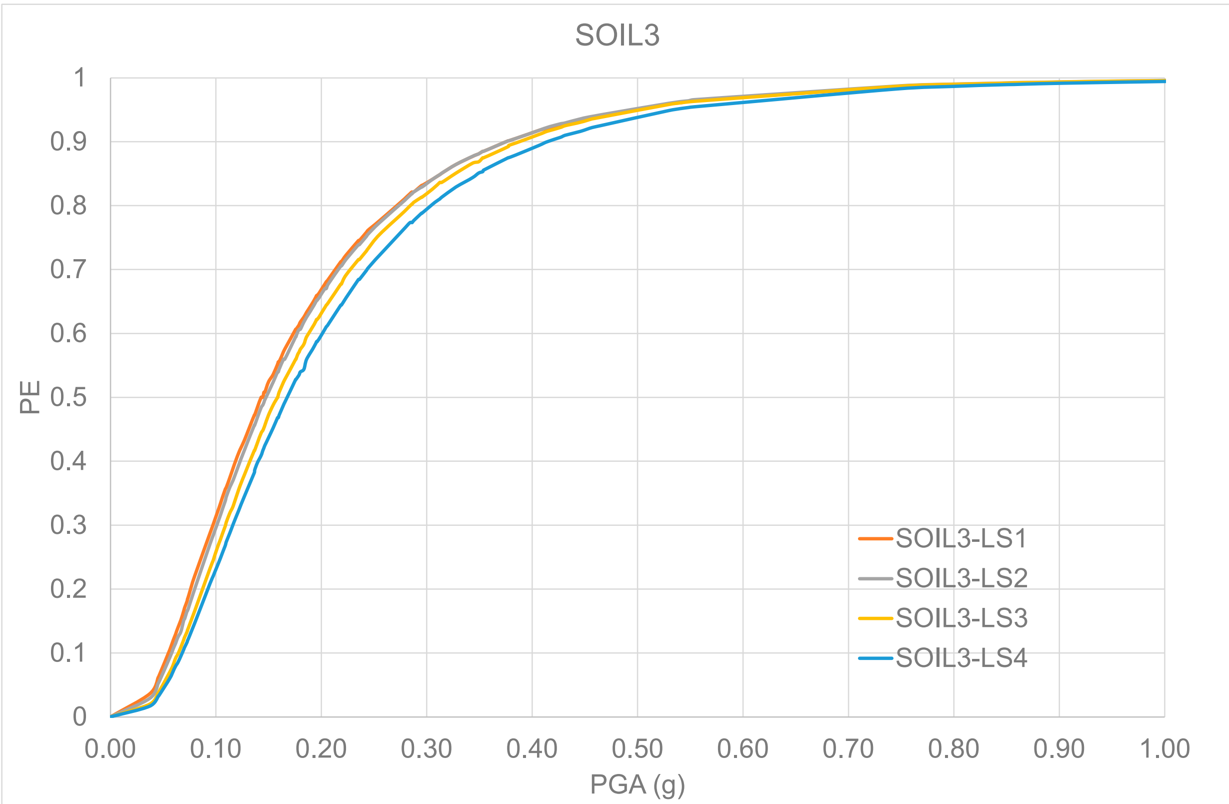

Figure 11. Fragility Curves: SOIL3.

Table 8. PE at PGA = 0.30 g for various soil conditions and limit states.

PGA = 0.30 g	LS1	LS2	LS3	LS4
SOIL1	0.77	0.73	0.70	0.68
SOIL2	0.80	0.78	0.72	0.70
SOIL3	0.84	0.83	0.81	0.79

Overall, the paper shows how the strains due to scenario 1 [6] may considerably be amplified when soil deformation is considered. It was shown that neglecting the SSI effects on the performance of the system (SOIL1 conditions) may considerably undervalue the pipeline vulnerability, leading to un-conservative predictions and designs. Even if the findings are limited to the considered conditions, they may be included in code provisions to consider the important contribution of SSI that is not considered due to the complexity connected with the design of pipelines founded on deformable soils. In addition, it is important to state that this paper models the soil with undrained conditions; future studies are required for considering the effects of the water that may severely modify the SSI effects, as shown in [50–52].

5. Conclusions

A 3D comprehensive (soil + pipeline) numerical model was herein proposed to consider the interaction between a non-linear soil and a steel pipeline (OD/t = 20) on a sleeper (h/OD = 1.97). Fragility curves were derived by performing 300 dynamic analyses with different soil conditions to define the probabilistic values (with linear regressions). The previous study [6] was used as a reference to calibrate the proposed FE model by considering a rigid soil (SOIL1, no SSI). The results show a good agreement, meaning that the model assumptions were properly defined. Then, the conditions of rigid soil were compared with deformable soil conditions (SOIL2 and SOIL3). The resulting smaller mean values with respect to those derived for SOIL1 demonstrated the importance of SSI in reducing the seismic vulnerability of the entire system (soil + pipeline). In particular, the non-linear behaviour of the soil was driven by the ultimate strength of the soil that needs a certain level of intensity to be mobilised. Therefore, the relative damage of the two soil conditions differs mainly at a moderate level of PGA, because such intensities may affect the soil in different ways. It was found that at a high level of PGA, the soil mobilises plastic behaviour affecting the performance of the soil-pipeline system. The most deformable soil (SOIL3) showed larger values of PE, demonstrating that SSI effects are detrimental. Overall, the paper showed how the strains due to scenario 1 [6] may considerably be amplified when soil deformation varies. It was shown that neglecting the SSI effects on the performance of the system (stiff soil conditions) may considerably undervalue the pipeline vulnerability, leading to un-conservative predictions and designs. The proposed case study may be considered a starting point for further works in this area. For example, the choice to use the PIMY model was aimed to focus on deformations due to soil deformability under undrained conditions. Other soil conditions and plastic effects will be the object of future studies. In addition, applications to other structures may assess the mutual behaviour of soil deformability and buckling under seismic scenarios.

Author Contributions: Conceptualisation, D.F. and H.K.; methodology, H.K. and D.M.; software, D.F.; validation, D.F., D.M. and H.K.; formal analysis, H.K.; investigation, D.M.; resources, D.F.; data curation, D.M.; writing—original draft preparation, D.F.; writing—review and editing, D.F.; visualisation, D.M.; supervision, H.K.; project administration, H.K.; funding acquisition, H.K. All authors have read and agreed to the published version of the manuscript.

Funding: This research received no external funding.

Institutional Review Board Statement: Not applicable.

Informed Consent Statement: Not applicable.

Conflicts of Interest: The authors declare no conflict of interest.

References

1. Yun, H.; Kyriakides, S. On the beam and shell modes of buckling of buried pipelines. *Soil Dyn. Earthq. Eng.* **1990**, *9*, 179–193. [CrossRef]
2. Daiyan, N.; Kenny, S.; Phillips, R.; Popescu, R. Numerical investigation of oblique pipeline/soil interaction in sand. In Proceedings of the 8th International Pipeline Conference, IPC2010-31644, Calgary, AB, Canada, 4 April 2011.
3. Vazouras, P.; Karamanos, S.A.; Dakoulas, P. Mechanical behavior of buried steel pipes crossing active strike-slip faults. *Soil Dyn. Earthq. Eng.* **2012**, *41*, 164–180. [CrossRef]
4. Vazouras, P.; Dakoulas, P.; Karamanos, S.A. Pipe-soil interaction and pipeline performance under strike-slip fault movements. *Soil Dyn. Earthq. Eng.* **2015**, *72*, 48–65. [CrossRef]
5. Vazouras, P.; Karamanos, S.A.; Dakoulas, P. Finite element analysis of buried steel pipelines under strike-slip fault displacements. *Soil Dyn. Earthq. Eng.* **2010**, *30*, 1361–1376. [CrossRef]
6. Mina, D.; Forcellini, D.; Karampour, H. Analytical fragility curves for assessment of the seismic vulnerability of hp/ht unburied subsea pipelines. *Soil Dyn. Earthq. Eng.* **2020**, *137*, 106308. [CrossRef]
7. Triantafyllaki, A.; Papanastasiou, P.; Loukidis, D. Numerical analysis of the structural response of unburied offshore pipelines crossing active normal and reverse faults. *Soil Dyn. Earthq. Eng.* **2020**, *137*, 106296. [CrossRef]
8. Alrsai, M.; Karampour, H. Propagation buckling of pipe-in-pipe systems, an experimental study. In Proceedings of the Twelfth ISOPE Pacific/Asia Offshore Mechanics Symposium, Old Coast, Australia, 4–7 October 2016.
9. Binazir, A.; Karampour, H.; Sadowski, A.J.; Gilbert, B.P. Pure bending of pipe-in-pipe systems. *Thin-Walled Struct.* **2019**, *145*, 106381. [CrossRef]
10. Karampour, H.; Albermani, F.; Gross, J. On lateral and upheaval buckling of subsea pipelines. *Eng. Struct.* **2013**, *52*, 317–330. [CrossRef]
11. Karampour, H.; Albermani, F.; Major, P. Interaction between lateral buckling and propagation buckling in textured deep subsea pipelines. In Proceedings of the International Conference on Offshore Mechanics and Arctic Engineering, American Society of Mechanical Engineers, St. John's, NL, Canada, 31 May–5 June 2015; Volume 56499, p. V003T02A079.
12. Piran, F.; Karampour, H.; Woodfield, P. Numerical Simulation of Cross-Flow Vortex-Induced Vibration of Hexagonal Cylinders with Face and Corner Orientations at Low Reynolds Number. *J. Mar. Sci. Eng.* **2020**, *8*, 387. [CrossRef]
13. Stephan, P.; Love, C.; Albermani, F.; Karampour, H. Experimental study on confined buckle propagation. *Adv. Steel Constr.* **2016**, *12*, 44–54.
14. Seth, D.; Manna, B.; Shahu, J.T.; Fazeres-Ferradosa, T.; Pinto, F.T.; Rosa-Santos, P.J. Buckling Mechanism of Offshore Pipelines: A State of the Art. *J. Mar. Sci. Eng.* **2021**, *9*, 1074. [CrossRef]
15. Seth, D.; Manna, B.; Kumar, P.; Shahu, J.T.; Fazeres-Ferradosa, T.; Taveira-Pinto, F.; Rosa-Santos, P.; Carvalho, H. Uplift and lateral buckling failure mechanisms of offshore pipes buried in normally consolidated clay. *Eng. Fail. Anal.* **2021**, *121*, 105161. [CrossRef]
16. Joshi, S.; Prashant, A.; Deb, A.; Jain, S.K. Analysis of buried pipelines subjected to reverse fault motion. *Soil Dyn. Earthq. Eng.* **2011**, *31*, 930–940. [CrossRef]
17. Liu, A.; Hu, Y.; Zhao, F.; Li, X.; Takada, S.; Zhao, L. An equivalent-boundary method for the shell analysis of buried pipelines under fault movement. *Acta Seismol. Sin.* **2004**, *17*, 150–156. [CrossRef]
18. Liu, M.; Wang, Y.; Yu, Z. Response of pipelines under fault crossing. In Proceedings of the Eighteenth International Offshore and Polar Engineering Conference, Vancouver, BC, Canada, 6 July 2008.
19. Odina, L.; Tan, R. Seismic fault displacement of buried pipelines using continuum finite element methods. In Proceedings of the International Conference on Offshore Mechanics and Arctic Engineering, Honolulu, HI, USA, 16 February 2010.
20. Odina, L.; Conder, R.J. Significance of Lüder's plateau on pipeline fault crossing assessment. In Proceedings of the ASME 2010 29th International Conference on Ocean, Offshore and Arctic Engineering, OMAE2010-20715, Shanghai, China, 22 December 2010.
21. Kokavessis, N.; Anagnostidis, G. Finite element modelling of buried pipelines subjected to seismic loads: Soil structure interaction using contact elements. In Proceedings of the ASME Pressure Vessels and Piping Conference, Vancouver, BC, Canada, 23 July 2008.
22. Zhang, J.; Liang, Z.; Han, C.J. Buckling behavior analysis of buried gas pipeline under strike-slip fault displacement. *J. Nat. Gas. Sci. Eng.* **2014**, *21*, 921–928. [CrossRef]
23. Thebian, L.; Najjar, S.; Sadek, S.; Mabsout, M. Finite element analysis of offshore pipelines overlying active reverse fault rupture. In Proceedings of the International Conference on Offshore Mechanics and Arctic Engineering, Trondheim, Norway, 6–11 July 2017. [CrossRef]
24. Lillig, D.B.; Newbury, B.D.; Altstadt, S.A. The second ISOPE strain-based design Symposium—A review. In Proceedings of the International Society of Offshore & Polar Engineering Conference, Osaka, Japan, 21–26 June 2009.
25. Karamitros, D.K.; Bouckovalas, G.D.; Kouretzis, G.P. Stress analysis of buried steel pipelines at strike-slip fault crossings. *Soil Dyn. Earthq. Eng.* **2007**, *27*, 200–211. [CrossRef]
26. Shitamoto, H.; Hamada, M.; Okaguchi, S.; Takahashi, N.; Takeuchi, I.; Fujita, S. Evaluation of compressive strain limit of X80 SAW pipes for resistance to ground movement. In Proceedings of the Twentieth International Offshore and Polar Engineering Conference, Beijing, China, 20 June 2010.

27. Arifin, R.B.; Shafrizal, W.M.; Wan, B.; Yusof, M.; Zhao, P.; Bai, Y. Seismic analysis for the subsea pipeline system. In Proceedings of the ASME 2010 29th International Conference on Ocean, Offshore and Arctic Engineering, OMAE2010-20671, Shanghai, China, 22 December 2010.
28. Dyan, J.; Kyriakides, S. On the response of elastic-plastic tubes under combined bending and tension. *J. Offshore Mech. Arctic. Eng.* **1992**, *114*, 50–62.
29. Fazeres-Ferradosa, T.; Rosa-Santos, P.; Taveira-Pinto, F.; Vanem, E.; Carvalho, H.; Correia, J.A.F.D.O. Editorial: Advanced research on offshore structures and foundation design: Part 1. In Proceedings of the Institution of Civil Engineers—Maritime Engineering, Telford, UK, 19 December 2019. [CrossRef]
30. Fazeres-Ferradosa, T.; Rosa-Santos, P.; Taveira-Pinto, F.; Vanem, E.; Carvalho, H.; Correia, J.A.F.D.O. Editorial. In Proceedings of the Institution of Civil Engineers–Maritime Engineering, Telford, UK, 18 March 2020; Volume 173, pp. 96–99. [CrossRef]
31. Chen, R.; Wu, L.; Zhu, B.; Kong, D. Numerical modelling of pipe-soil interaction for marine pipelines in sandy seabed subjected to wave loadings. *Appl. Ocean Res.* **2019**, *88*, 233–245. [CrossRef]
32. Ghorbani, J.; Nazem, M.; Kodikara, J.; Wriggers, P. Finite element solution for static and dynamic interactions of cylindrical rigid objects and unsaturated granular soils. *Comput. Methods Appl. Mech. Eng.* **2021**, *384*, 113974. [CrossRef]
33. Chatterjee, S.; White, D.J.; Randolph, M.F. Numerical simulations of pipe-soil interaction during large lateral movements on clay. *Geotechnique* **2012**, *62*, 693–705. [CrossRef]
34. Mazzoni, S.; McKenna, F.; Scott, M.H.; Fenves, G.L. *Open System for Earthquake Engineering Simulation, User Command-Language Manual*; OpenSees Version 2.0; Pacific Earthquake Engineering Research Center, University of California: Berkeley, CA, USA, 2009. Available online: http://opensees.berkeley.edu/OpenSees/manuals/usermanual (accessed on 22 December 2021).
35. Lu, J.; Elgamal, A.; Yang, Z. *OpenSeesPL: 3D Lateral Pile-Ground Interaction User Manual (Beta 1.0)*; Department of Structural Engineering, University of California: San Diego, CA, USA, 2011.
36. Forcellini, D. Soil-structure interaction analyses of shallow-founded structures on a potential-liquefiable soil deposit. *Soil Dyn. Earthq. Eng.* **2020**, *133*, 106108. [CrossRef]
37. Forcellini, D. Probabilistic-Based Assessment of Liquefaction-Induced Damage with Analytical Fragility Curves. *Geosciences* **2020**, *10*, 315. [CrossRef]
38. Forcellini, D. Analytical fragility curves of shallow-founded structures subjected to Soil-Structure Interaction (SSI) effects. *Soil Dyn. Earthq. Eng.* **2021**, *141*, 106487. [CrossRef]
39. Forcellini, D. A Resilience-Based Methodology to Assess Soil Structure Interaction on a Benchmark Bridge. *Infrastructures* **2020**, *5*, 90. [CrossRef]
40. Karampour, H.; Wu, Z.; Lefebure, J.; Jeng, D.S.; Etemad-Shahidi, A.; Simpson, B. Modelling of flow around hexagonal and textured cylinders. *Proc. Inst. Civ. Eng. Eng. Comput. Mech.* **2018**, *171*, 99–114. [CrossRef]
41. Karampour, H. Effect of proximity of imperfections on buckle interaction in deep subsea pipelines. *Mar. Struct.* **2018**, *59*, 444–457. [CrossRef]
42. Taiebat, M.; Dafalias, Y.F. SANISAND: Simple anisotropic sand plasticity model. *Int. J. Numer. Anal. Methods Geomech.* **2008**, *32*, 915–948. [CrossRef]
43. Ghorbani, J.; Airey, D.W.; Carter, J.P.; Nazem, M. Unsaturated soil dynamics: Finite element solution including stress-induced anisotropy. *Comput. Geotech.* **2021**, *133*, 104062. [CrossRef]
44. Pestana, J.M.; Whittle, A.J. Formulation of a unified constitutive model for clays and sands. *Int. J. Numer. Anal. Methods Geomech.* **1999**, *23*, 1215–1243. [CrossRef]
45. Ghorbani, J.; Airey, D.W. Modelling stress-induced anisotropy in multi-phase granular soils. *Comput. Mech.* **2021**, *67*, 497–521. [CrossRef]
46. Dafalias, Y.F.; Taiebat, M. SANISAND-Z: Zero elastic range sand plasticity model. *Géotechnique* **2016**, *66*, 999–1013. [CrossRef]
47. Jeremić, B.; Cheng, Z.; Taiebat, M.; Dafalias, Y. Numerical simulation of fully saturated porous materials. *Int. J. Numer. Anal. Methods Geomech.* **2008**, *32*, 1635–1660. [CrossRef]
48. *Offshore Standard*; DNV-OS-F101 Submarine Pipeline Systems; DET NORSKE VERITAS: Bærum, Norway, 2007.
49. Tsiavos, A.; Amrein, P.; Bender, N.; Stojadinovic, B. Compliance-based estimation of seismic collapse risk of an existing reinforced concrete frame building. *Bull. Earthq. Eng.* **2021**, *19*, 6027–6048. [CrossRef]
50. Khosravikia, F.; Mahsuli, M.; Ghannad, M.A. The effect of soil—Structure interaction on the seismic risk to buildings. *Bull. Earthq. Eng* **2018**, *16*, 3653–3673. [CrossRef]
51. Cavalieri, F.; Correia, A.A.; Crowley, H.; Pinho, R. Dynamic soil-structure interaction models for fragility characterisation of buildings with shallow foundations. *Soil Dyn. Earthq. Eng.* **2020**, *132*, 106004. [CrossRef]
52. Forcellini, D. The Role of the Water Level in the Assessment of Seismic Vulnerability for the 23 November 1980 Irpinia–Basilicata Earthquake. *Geosciences* **2020**, *10*, 229. [CrossRef]